Chapter

Thermoluminescence Dosimetry Technique for Radiation Detection Applications

Hossam Donya

Abstract

Due to the risk of radiation exposure, radiation dosimetry is performed regularly to ensure the occupational safety of personnel and radiation workers. Therefore, various dosimeters are widely used to detect neutrons, gamma, X-ray, and proton irradiation fields. As an example, in medical applications, routine personal dosimetry is used to monitor and limit workers' long-term occupational exposure. Radiation workers who undertake X-ray diagnostic, radiotherapy operations, in clinical and industrial application. Although, the overheads of running an in-house TLD (Thermoluminescent dosimetry) service for monitoring doses to eyes, pacemakers and so on seems rather high for the benefits conferred, however, it is still widely used for reporting doses accurately in various medical centers over the world. TLD also is widely used for measuring entrance doses on a handful of patients to validate a new LINAC/TPS combination. As well as in the industrial field as if petroleum, companies or nuclear reactor, RSO (radiation safety officer) used TLD badges to report delivered doses. In this chapter, we focus on the TLD technique for measuring doses of various ionizing radiation detection. Different methods for evaluations of TL Kinetics are covered. Modern TLD applications in the clinical field are also investigated. Some recommendations on advance dosimetry failure of TLD are concluded.

Keywords: TLD, TL kinetics, radiotherapy, hybrid-functional density theory, modern clinical applications

1. Introduction

TLD method is considered an important technique as it can store radiation in trap centers for long period. Glow peaks of thermoluminescence dosimeters are later measured and discussed based on some models related to the physical changes in the band structure of dosimeter because of ionizing radiation exposure. A wide range of substances exhibits thermoluminescence (TL) phenomena after being exposed to nuclear radiation such as activated LiF and CaSO4. Thermoluminescent dosimeter (TLD) emits light when heated up after being irradiated. Due to this special property, TLD could be used as a radiation dosimeter. TLD has many advantages and sensitive to different types of radiation. A dosimeter of higher TL response to thermal neutrons

is most commonly used in mixed radiation fields (neutron and gamma ray). The sensitivity of TLD to neutrons depends on the detector compound type, environment and neutron energy. For neutron dosimetry purposes, the neutron and gamma ray dose contribution must be separated by using two different detector types of TLD. The first one should be sensitive to gamma and the other should be sensitive to neutrons plus gamma (as LiF-700 and LiF-600) [1, 2].

The response of fast neutrons depends on the cross-section for the interaction in TLD material and the relative TL efficiency, which depends on the linear energy transfer (LET) of the reaction products in the first place. The response to intermediate-energy depends mainly on the cross-section of the reaction, which may take place with the composite material of the TLD.

1.1 TLD applications in neutron and gamma ray dosimetry

Generally, there are three types of TLD used for neutron dosimetry as follow:

1.1.1 Albedo neutron dosimeter

A considerable fraction of intermediate and fast neutrons can be slowed down to epithermal neutron energy and backscattered in the human body, interacting with the sensitive TL material. An albedo neutron dosimeter is a type of neutron monitor and is typically used in the neutron energy range of 0.2 eV to around 0.5 MeV. The slow neutrons interact with TL material, usually through ^{6}Li (n,α) 3H reaction, and the resulting induced charged particles to stimulate the TL material. Recently, some of albedo TLD dosimeters depend on ^{10}B (n, α) 7Li reactions. Because neutron TL sensitive material responds to gamma radiation, and neutrons are accompanied by this gamma radiation, another TLD is usually utilized in conjunction with TLD with a gamma ray.

The neutron albedo dosimeter measures (a) direct fast neutrons, (b) direct thermal neutrons, and (c) albedo neutrons reflected from the body. This type of dosimeter uses Lexan polycarbonate and/or CR-39 foils, as well as two 10B (n, γ) ^{7}Li converters in a cadmium cover, to efficiently measure the three neutron dosage components independently [3–5]. Fast neutron dose is assessed in CR-39 by counting proton recoil tracks, while thermal neutron dose is determined by counting α particles created during the process. Because the albedo dosimeter has a sensitivity range of 0.3–30 mSv, it is advised that it be used as a backup dosimeter to assist in the assessment of high dose values in the event of accidents or patients receiving neutron therapy.

In another application, the ^{10}B (n, α) ^{7}Li reactions with the backscattered albedo neutrons employed with Electret's ionization chamber proposed by Seifert et al. [6, 7]. In this chamber, induced ^{7}Li from the ionization of the gas in the chamber worn on the body's surface in the above reaction instance. Under saturation conditions, produced charge carriers with the corresponding polarity travel to the surface of the electret. As a result, the change in the electrets voltage is a direct measure of albedo neutron fluence and an indirect estimate of primary neutron fluence. In general, the advantages of albedo TLD dosimeter are: they are relatively inexpensive and can be reused, easily fabricated, lightweight to wear, Readout is simple and can be automated, Insensitive to humidity.

While their disadvantages are: Some of TLD exhibit fading, TLD is sensitive to gamma-ray, they must be worm properly or serious errors can be resulted, the

measured values of TLD does not give permanent record as the track detectors, their sensitivity is highly dependent on the angle and energy of incidence radiation.

1.1.2 Hydrogenous radiator TLDs

In this type of dosimeters, the fast neutrons knock out protons from hydrogenous material mixed with the phosphor, and the protons dispel their energy in the dosimeter. In this method, the hydrogenous substances are called proton radiators [8]. This technique has demonstrated that TL materials mixed with hydrogenous material can detect fast neutrons, but the sensitivity needs to be improved by one order of magnitude before using in personnel neutron dosimetry.

1.1.3 LET-dependent deep trap TLD glow peaks

The fast neutron interacts directly with the TL material as calcium fluoride (CaF_2: Tm) which is commercially called TLD-300. This type has a glow curve with two glow peaks and the peak temperature T_m centered 150 and 250°C, respectively. The higher temperature peak (250°C) has a greater response to the fast neutrons. TLD-300 dosimeter CaF_2: Tm (0.35 Mol. %) showed a lower detection limit of about 0.3 mSv from [241]Am-Be source.

2. Characteristic of TLD phosphors

2.1 The glow curve

The term "Glow curve" refers to the graph of TL as a function either of temperature or of time as shown in **Figure 1**.

Glow curves have the following features:-

- The glow curve of a certain phosphor probably best characterizes that phosphor. For example, the appearance of glow peaks only at low temperatures implies that the phosphor loses its stored TL with time, and therefore would be unsuitable for long-term measurements.
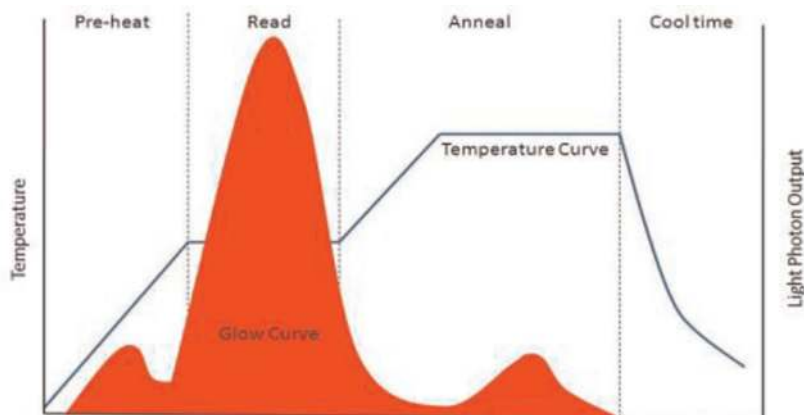

Figure 1.
TLD glow curve and time–temperature profile (TTP).

- A peak at very high temperatures indicates a phosphor that will produce infrared radiation at the temperature necessary to release the TL. This is a problem for the instrumentation.

- A glow curve without well-defined peaks makes the selection of the appropriate end for integration difficult. Ideally then, a glow curve should reveal only a single thermoluminescent peak, which occurs at a temperature high enough to ensure room temperature stability but not so high as to present instrumental problems. However, the temperature at which a TL peak appears is quite affected by the heating rate.

The following factors may affect the shape of the glow curve:

2.2 TL sensitivity

The sensitivity of TLD should be evaluated for competitor's materials to determine the dose linearity, sub linearity or supralinearity behavior of phosphors. The sensitivity and thermal stability of glass samples were found to be dependent on both the starting materials and the method of preparation in Refs. [9–13].

2.3 Dose rate dependence

TL dosimeters, in general, have demonstrated no dose rate effects over a wide range.

2.4 Stability

TL is the release, in the form of visible light, of energy absorbed from previous irradiation. The rate at which this energy is released is dependent upon the phosphor temperature and increases sharply at a higher temperature. Even though the concept of "glow peak temperature" that temperature at which the maximum of the glow peak occurs, is both useful and easily demonstrated. It should be remembered that a finite rate of loss of stored energy exists even for much lower temperatures. If a phosphor shows an insignificant loss of TL at room temperature, it is said to have good stability.

3. TL kinetics

The physical process leading to the emission of TL from a sample is related in most cases to the traffic of charge carriers, usually electrons and holes, between different imperfection states in the solid sample. Studying the kinetics of the TL process means the investigation of electron–hole transitions between energy states in cases of both the irradiation of the TL sample and the readout processes. Although, in most experimental situations the TL curve consists of several overlapping peaks, it is appropriate to start the discussion by dealing with a single peak to understand the basic process. For most purposes, it is not necessary to assume that the glow curve consists of only one peak. The analysis of a single peak may just be valid if a series of peaks occur, provided that the peak of interest is sufficiently separated from others, either because it appears separately or because we have an efficient method to isolate it from the rest of the curve.

3.1 First kinetics order

If n is the number of trapped electrons in the sample, which is maintained at constant temperature T, n decreases with time t as:

$$\frac{-\mathrm{d}n}{\mathrm{d}t} = P\,n \tag{1}$$

From Eq. (1) we get:

$$\frac{-\mathrm{d}n}{\mathrm{d}t} = nS \exp\left(\frac{-E}{KT}\right) \tag{2}$$

The rate of photon emission, and hence the rate of release of electrons from traps to their rate of arrival at luminescence centers, determine the strength of the TL glow peak [14].

$$I\alpha - \frac{\mathrm{d}n}{\mathrm{d}t} \rightarrow I = -C\frac{\mathrm{d}n}{\mathrm{d}t} = nCS \exp\left(\frac{-E}{KT}\right) \tag{3}$$

Where C is a luminescence efficiency constant.
When the dosimeter is heated with rate $\beta = \mathrm{d}T/\mathrm{d}t$. Then we may write $\mathrm{d}n/\mathrm{d}t$ as:

$$\frac{\mathrm{d}n}{\mathrm{d}t} = \frac{\mathrm{d}n}{\mathrm{d}T}\frac{\mathrm{d}T}{\mathrm{d}t} = \beta\frac{\mathrm{d}n}{\mathrm{d}T} \tag{4}$$

Substitute in Eq. (2), we get:

$$\rightarrow \frac{\mathrm{d}n}{\mathrm{d}T} = \frac{-nS}{\beta} \exp\left(\frac{-E}{KT.}\right)$$

$$\rightarrow \int_{n_o}^{n} \frac{\mathrm{d}n}{n} = \frac{-S}{\beta} \int_{T_o}^{T} \exp\left(\frac{-E}{KT}\right)\mathrm{d}T$$

Where n_o denotes the number of electrons in the trap at a given time and temperature, t_o and T_o, respectively.

$$n = n_o \exp\left(\frac{-S}{R} \int_{T_o}^{T} \exp\left(\frac{-E}{KT}\right)\mathrm{d}T\right) \tag{5}$$

Substitute in Eq. (3)

$$I = n_o SC \exp\left(\frac{-E}{KT}\right) \exp\left(\frac{-S}{\beta} \int_{T_o}^{T} \exp\left(\frac{-E}{KT}\right)\mathrm{d}T\right) \tag{6}$$

It should be noted that $I(T)$ in Eq. (6) dependents on two physical parameters, the activation energy E, and frequency factor S, and the heating rate β. The activation energy is the minimum energy required to release the electrons from their traps. Differentiation of Eq. (6) with respect to the temperature gives:

$$\frac{\partial I}{\partial T} = n_o SC\left\{ \exp\left(\frac{-E}{KT}\right) \exp\left(f(T)\right)\frac{\partial f(T)}{\partial T} + \exp\left(f(T)\right)\exp\left(\frac{-E}{KT}\right)\left(\frac{E}{KT^2}\right)\right\}$$

Where, $f(T) = \frac{-S}{\beta} \int^{T} \exp\left(\frac{-E}{KT}\right) dT$

At $T = T_m \rightarrow \frac{\partial I}{\partial T} = 0$

$$\rightarrow \frac{s}{\beta} \exp\left(\frac{-E}{KT_m}\right) = \frac{E}{KT_m^2} \qquad (7)$$

where T_m is peak position or the temperature at maximum intensity.

Equation (7) describes the condition of the occurrence of the maximum intensity and the determination of the corresponding temperature, which we call, T_m. The reduction in the second exponential function is faster than the growth in the first exponential function above this temperature, and the product function decreases until the traps are fully depopulated. This accounts for the end of the peak. A theoretical (calculated) glow peak plotted using Eq. (6) is shown in **Figure 2**. The main feature of the first-order peak is that the asymmetric, is such that at temperatures over T_m, the reduction is faster than the rise at low temperatures.

The initial concentration n_o appears in the first kinetics order acts only as a constant multiplying the temperature-dependent factors. In this particular case of the first kinetics order, changing the initial concentration n_o has no effect on the curve's form because adjusting the intensity at each temperature has the same proportional effect. **Figure 3** shows several glow peaks with different n_o. One of the aspects of this fact is that T_m is independent of the initial concentration n_o.

This appears well in the condition of the T_m described by Eq. (7), where n_o does not appear in the equation. This property of the independent of T_m on n_o is specified to the first-order case, and will not occur for most of the other kinetics possibilities [13]. Eq. (7) can be written in the following form:

$$\frac{\beta E}{K} = ST_m^2 \exp\left(\frac{-E}{KT_m}\right) \qquad (8)$$

We see that changing the heating rate β must change T_m in a such way that equality still holds. The term $T_m^2 \exp\left(\frac{-E}{KT}\right)$ is monotonically increasing with T_m, therefore increasing the rate β will immediately cause T_m to increase. Since $T_m^2 \exp\left(\frac{-E}{KT}\right)$ is a very rapidly increasing function of T_m, only a small change of T_m may accompany a large variation in the heating rate β, this variation is usually rather easily observable.
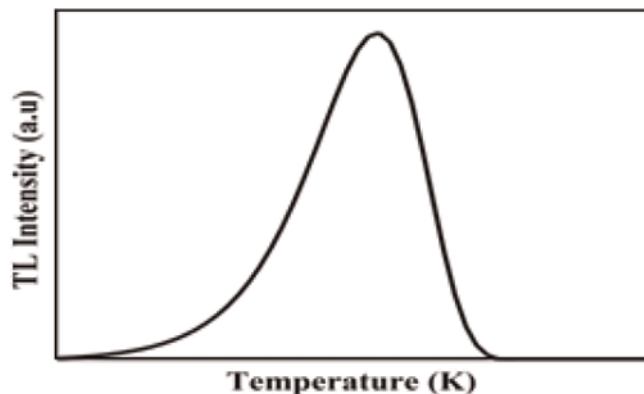

Figure 2.
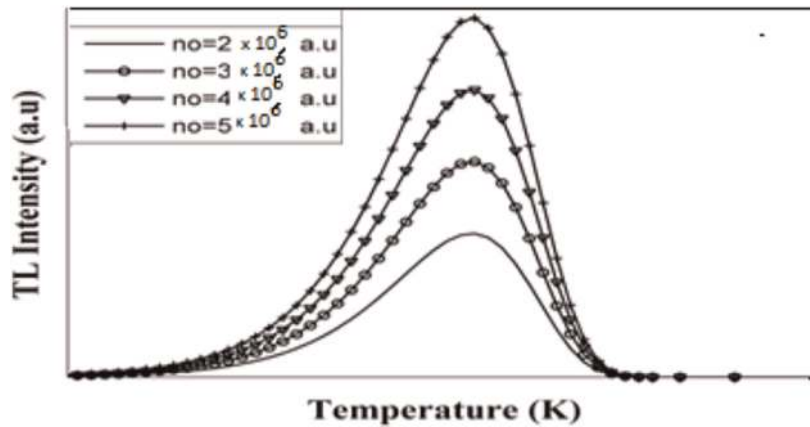*Theoretical glow peak plotted using the first kinetics order equation.*

Figure 3.
Glow curves plotted using the first-order kinetics equation for different n_o.

3.1.1 Second kinetics order

One assumption made up by Randall and Wilkins [14] which led to the first kinetics order was that once a charge carrier is thermally elevated into the band, it is bound to recombine rather quickly with an opposite sign carrier trapped in a recombination center. Gralick and Gibson [15] considered another case in which the free carriers may re-trap with equal retrapping recombination probabilities with the further assumption that the concentration of electrons in traps and holes in recombination centers are equal during the entire process. Denoting the total number of traps of the given type (free electrons or holes) by N, they found the kinetics equation:

$$I = \frac{-dn}{dt} = \left(\frac{S}{N}\right)n^2 \exp\left(\frac{-E}{KT}\right) \tag{9}$$

where (S/N) is a constant having units of $m^3 s^{-1}$, which we may denote by S'. Then we have

$$I = \frac{-dn}{dt} = S'n^2 \exp\left(\frac{-E}{KT}\right) \tag{10}$$

where S' is called "pre-exponential factor" which does not have the same meaning of "frequency factor" as was in the first kinetics order.

For linear heating rate β, we have:

$$I = \frac{-dn}{dt} = \frac{-dn}{dT} \underset{\rightarrow}{\text{yields}} \frac{dn}{dT} = \frac{-\acute{S}}{\beta}n^2 \exp\left(\frac{-E}{KT}\right)$$

$$\underset{\rightarrow}{\text{yields}} \frac{1}{n} - \frac{1}{no} = \frac{\acute{S}}{-}\int^T \exp\left(\frac{-E}{KT}\right)dT$$

$$\underset{\rightarrow}{\text{yields}} n = n_o\left\{1 + \left(\frac{\acute{S}}{-}\right)n_o\int^T \exp\left(\frac{-E}{KT}\right)dT\right\}^{-1} \tag{11}$$

Substitute in Eq. (10),

$$I = \acute{S}n_o^2 \exp\left(\frac{-E}{KT}\right)\left\{1 + \left(\frac{\acute{S}}{}\right)n_o \int^T \exp\left(\frac{-E}{KT}\right)dT\right\}^{-2} \tag{12}$$

where Eq. (12) represents the intensity of a glow peak according to the second kinetics order model. At high temperature, the second decreasing function dominates so that the product function is decreasing. Somewhere between two regions the glow curve, therefore, reaches its maximum. **Figure 4** Displays a hypothetical glow peak plotted using Eq. (12).

The condition of the maximum is found by setting the derivative of Eq. (12) to zero (dI/dT = zero) [16], then we may find:

$$\frac{dI}{dT} = \acute{S}n_o^2 \left\{\begin{array}{l} -2\,exp\left(\frac{-E}{KT}\right)\left\{1 + \left(\frac{\acute{S}n_o}{\beta}\right)\int^T \exp\left(\frac{-E}{KT}\right)dT\right\}^{-3}\left(\left(\frac{\acute{S}n_o}{\beta}\right)\exp\left(\frac{-E}{KT}\right)\right) \\ +E/KT^2 \exp\left(\frac{-E}{KT}\right)\left\{1 + \left(\frac{\acute{S}n_o}{\beta}\right)\int^T \exp\left(\frac{-E}{KT}\right)dT\right\}^{-2} \end{array}\right\}$$

$$\frac{dI}{dT} = 0\, at\, T = T_m \underset{\rightarrow}{yields} \frac{2\acute{S}n_o}{\beta}\exp\left(\frac{-2E}{KT_m}\right)\left\{1 + \left(\frac{\acute{S}n_o}{\beta}\right)\int^{T_m} \exp\left(\frac{-E}{KT_m}\right)dT\right\}^{-3}$$

$$\frac{E}{KT_m^2}\exp\left(\frac{-E}{KT_m}\right)\left\{1 + \left(\frac{\acute{S}n_o}{\beta}\right)\int^{T_m} \exp\left(\frac{-E}{KT_m}\right)dT\right\}^{-2}$$

Multiply by $\left\{1 + \left(\frac{\acute{S}}{\beta}\right)no\int^{T_m} \exp\left(\frac{-E}{KT_m}\right)dT\right\}^3$ and rearrange, one gets

$$\left\{1 + \left(\frac{\acute{S}}{\beta}\right)no\int^{T_m} \exp\left(\frac{-E}{KT_m}\right)dT\right\} = \frac{2KT_m^2\acute{S}n_o}{\beta E}\exp\left(\frac{-E}{KT_m}\right) \tag{13}$$

Then Eq. (13) represents the condition of the peak maximum according to the second kinetics order. As can see n_o appears in the equation and therefore we expect that T_m will depend on n_o. It can be shown numerically or analytically, that increasing
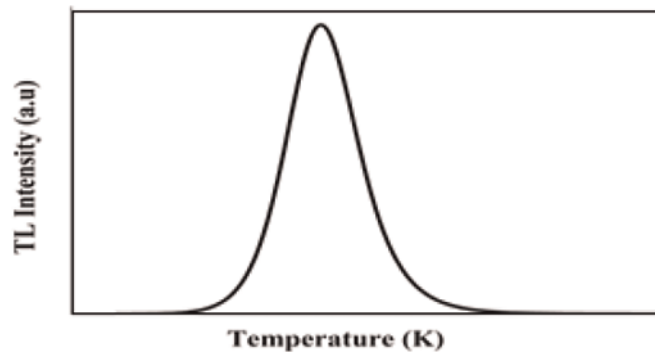

Figure 4.
Theoretical glow peak plotted using the second-order kinetics equation.

n_o causes T_m to decrease. An exception to this rule of the shift of a second-order peak with n_o can be found by Wrzesinska [17], who writes Eq. (10) with $S' = \frac{S}{n_o}$. The resulting peak has all the regular features of a second-order peak (e.g., symmetry properties) except one can write S instead of n_oS' and thus Eq. (10) turns out to be independent of n_o. The ensuring T_m is, therefore independent of n_o. It is not clear, however, what physical circumstances result in S' being equal to S/n_o [17]. Other aspects of the dependence of the glow curve on the initial concentration n_o are paramount importance when we are interested in a TL as a dosimetric tool. In many cases, one associated the initial concentration with the imparted dose and then the dependence of different parts of the glow peak on n_o is important. In the first kinetics order, since the intensity at each point is multiplied by the same factor while changing n_o, the total area varies with the same amount so that the total area is proportional to n_o. Its occurrence in second-order peak can be illustrated by integrating Eq. (9) with respect to time from zero to infinity;

$$\int_0^\infty I(t)\mathrm{d}t = -\int_{n_o}^n \mathrm{d}n = n_o - n_\infty = n_o \qquad (14)$$

Both in the first order and second order, as well as other cases, n_∞ is zero and therefore the integral, which represents the area under the glow peak is equal (in appropriate units) to n_o.

Now we can consider the dependence of different portions of the second-order peak on n_o. First, we shall study the dependence of I on n_o for a given temperature T. In the initial rise range, Eq. (12) reduces to:

$$I(T) \cong n_o^2 S' \exp\left(\frac{-E}{KT}\right) \qquad (15)$$

This shows immediately that for a given temperature in this range the dependence of I on n_o is superlinear, namely $I \, \alpha \, n_o$. It is to be emphasized that it is true only in the initial rise region; as already shown the total area is proportional to n_o and different dependencies are expected on other portions of the curve. Using the maximum condition equation and approximation to $\int^T \exp\left(-E/KT\right)\mathrm{d}T$, it can be shown that the two terms in the brackets in Eq. (12), namely unity and $n_o \frac{S'}{\beta} T_o \exp\left(-E/KT\right)\mathrm{d}T$ are more or less equal at $T = T_m$. At higher temperature, the latter term increases substantially and the unity can be neglected so that we obtain:

$$I \cong S'no^2 \exp\left(\frac{-E}{KT}\right)\left\{\left(\frac{S'}{\beta}\right)no\int^T exp\left(\frac{-E}{KT}\right)\mathrm{d}T\right\}^{-2}$$

$$\underset{\rightarrow}{\text{yieldsI}} \cong S' \exp\left(\frac{-E}{KT}\right)\left\{\left(\frac{S'}{\beta}\right)\int^T \exp\left(\frac{-E}{KT}\right)dT\right\}^{-2} \qquad (16)$$

The main point in Eq. (18) is that the term includes n_o cancel. This means that at a higher temperature range the TL intensity is independent of n_o for any given temperature [17].

Figure 5 shows plotted glow peaks using Eq. (12) for different n_o. In the low-temperature range, the TL intensity appears to depend on n_o. As n_o increases, T_m decreases which makes the peaks appear to be shifted to the low-temperature side. As

the temperature increases the effect of n_o on the peak starts to decrease which makes the peaks approach each other's on the high-temperature side.

3.1.2 A single TL peak analysis

As seen in **Figure 6**, the concentration of the trapping state is denoted by N (m^{-3}), with $n(t)$ (m^{-3}) being filled by electrons at time t(s). These electrons can be thermally elevated into the conduction band by crossing an energy barrier of E (eV) at a rate proportional to exp.$(-E/kT)$, resulting in a concentration of free electrons $n_c(t)$ (m^{-3}). Following that, these can be retrapped in a similar trap with a re-trapping probability A_n or recombined with a trapped hole in a center with a recombination center probability A_m, generating a photon with the recombination center energy h. A set of three simultaneous differential equations governs this operation. The following factors influence the recombination process:

$$I \alpha n_c m \text{ myields} I \xrightarrow{} = \frac{-\mathrm{d}m}{\mathrm{d}t} = A_m n_c m \tag{17}$$

where n, m, and n_c are the trapped electron, hole in the center, and free-electron concentrations, respectively, and $(\mathrm{d}m/\mathrm{d}t)$ is the recombination rate. This means that the amount of light emitted is proportional to the pace at which m decreases. The rate of recombination is proportional to both the instantaneous concentration of free
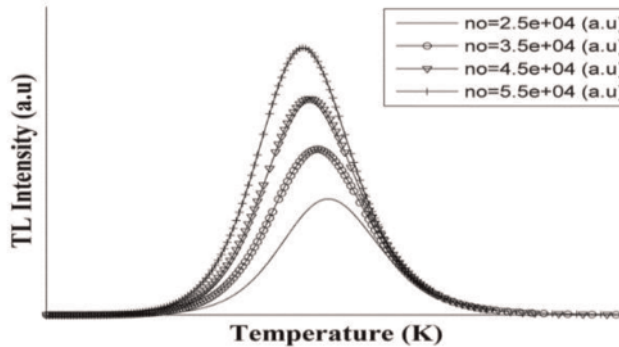

Figure 5.
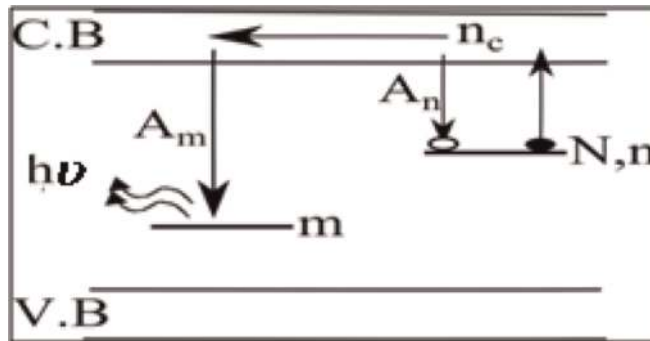*Plotted glow peaks using the second-order kinetics equation for different* n_o.

Figure 6.
A general treatment of the charge carriers' transitions in the TL sample.

electrons n_c and the concentration of hole centers m, the proportional constant Am (m^3 s^{-1}). The product of cross-section recombination σ (m^2) and thermal velocity is commonly used to calculate this value (m.s^{-1}). The second equation is concerned with the movement of electrons that have been thermally liberated from the trapped condition. The rate of release of these electrons –dn/dt is proportional to the trapped electron concentration n (m^{-3}) and the Boltzman constant exp.($-E$/KT), with S serving as the proportional constant (s^{-1}).

However, the actual rate of change of n is also related to the retraping term. The rate of retraping is proportional to the concentration of free electrons n_c, and the unoccupied trapping states *N-n*, the proportional factor being the recombination probability A_n(m^{3}s^{-1}). Thus, the second combined equation is given by:

$$\frac{-\mathrm{d}n}{\mathrm{d}t} = Sn \exp\left(\frac{-E}{KT}\right) - A_n n_c(N - n) \tag{18}$$

The third equation is that of charge neutrality. In its simplest form, it should read *m = n + n_c*. Taking the first derivative with respect to time, the charge neutrality condition can be written as:

$$\frac{\mathrm{d}m}{\mathrm{d}t} = \frac{\mathrm{d}n}{\mathrm{d}t} + \frac{\mathrm{d}n_c}{\mathrm{d}t} \tag{19}$$

$$\text{yields} \underset{\rightarrow}{} \frac{\mathrm{d}n_c}{\mathrm{d}t} = Sn \exp\left(\frac{-E}{KT}\right) - n_c\{mA_m + (N - n)A_n\} \tag{20}$$

This equation has been given by Adirovitch [18] for phosphorescence and by Halperin and Braner [19].

Now let us discuss the kinetics of the process in more general terms and see how the simplified cases of first, second, and more general cases emerge from Eqs. (17)–(20). Two simplifying assumptions were first made by Adirovitch [18] and later by many other investigators [19–23]. These are related to the relation between the concentration of the electrons in the conduction band and in traps and to the rate of change of these concentrations, namely:

$$\left|\frac{\mathrm{d}d}{\mathrm{d}t}\right| \ll \left|\frac{\mathrm{d}n}{\mathrm{d}t}\right|, n_c \ll n \tag{21}$$

Although, it seems to be the same connection between these two conditions, basically they are two separate relations and the occurrence of one does not necessarily imply the other. With these assumptions, Helperin and Braner [19] found the expression:

$$I = \frac{-\mathrm{d}m}{\mathrm{d}t} = \frac{mA_m}{mA_m + A_n(N - n)} Sn \exp\left(\frac{-E}{KT}\right) \tag{22}$$

Since this equation contains two unknown functions, $n(t)$ and $m(t)$, it cannot be solved without further assumption. As mentioned, Randall and Wilkins [14] wrote their first-order equation assuming strong recombination. This can be expressed in more specific terms. If we assume with relation to Eq. (22) that:

$$mA_m \gg (N - n)A_n$$

The condition of Eq. (22) is the relation between functions rather than parameters. It is, therefore, possible that at the low-temperature range of a glow peak, the strong inequality holds, and at higher temperatures where m and n decreases, the inequality "weakens" may be inverted. This may result in a shift from first-order behavior to non-first-order behavior within the same peak [24].

Then, one can say that:

$$mA_m + (N - n)A_n \cong mA_m \underset{\rightarrow}{\text{yields}} \frac{mA_m}{mA_m + A_n(N - n)} \cong 1$$

Then Eq. (22) will take the following form:

$$I = \frac{-\mathrm{d}m}{\mathrm{d}t} = Sn \exp\left(\frac{-E}{KT}\right) \tag{23}$$

Then we see that Eq. (23) takes the same form of Eq. (3). For linear heating rate function, the general solution of Eq. (23) is given by Eq. (24):

$$I = noS \exp\left(\frac{-E}{KT}\right) \exp\left(\frac{-S}{\beta}\int^T \exp\left(\frac{-E}{KT}\right)\mathrm{d}T\right) \tag{24}$$

Then from Eq. (22) with Randall and Wilkins [14] assumptions, we reached the first kinetics order equation.

The abovementioned second kinetics order, resulting from different assumptions associated with Eq. (22). In one set of assumptions, one can take $n(t) = m(t)$ which is not very different from the parametric equality $n_o = m_o$ once the assumption $n_c \ll n$ is made.

In addition, we have to assert the retraping dominates [15]

$$A_n(N - n) \gg mA_m \tag{25}$$

We also suppose that the trap is far from being saturated, i.e., the retrapping duration.

$$n \ll N \tag{26}$$

Then, from Eq. (26) one can write:

$$\frac{mA_m}{mA_m + A_n(N - n)} \simeq \frac{mA_m}{A_n(N - n)} \tag{27}$$

Using the condition of Eq. (26) in Eq. (27) one gets:

$$\frac{mA_m}{mA_m + A_n(N - n)} \simeq \frac{mA_m}{A_n(N - n)} \simeq \frac{mA_m}{NA_n} \tag{28}$$

and since we have assumed that $n(t) = m(t)$,

$$\frac{mA_m}{mA_m + A_n(N - n)} \simeq \frac{mA_m}{A_n(N - n)} \simeq \frac{mA_m}{NA_n} \simeq \frac{nA_m}{NA_n} \tag{29}$$

Then, apply to Eq. (22), we get:

$$I = \frac{-\mathrm{d}m}{\mathrm{d}t} = \frac{A_m S}{A_n N} n^2 \exp\left(\frac{-E}{KT}\right) \qquad (30)$$

Alternatively, one can assume, in addition to the concentration equality, that $A_n = A_m$ [18] which yields:

$$I = \frac{-dm}{dt} = \frac{S}{N} n^2 \, exp\left(\frac{-E}{KT}\right) \qquad (31)$$

Then Eq. (22) takes the same form of Eq. (8) which is found by Gralick and Gibson [15]. Where Eq. (30) sums up both these possibilities by employing the parameter S' ($m^3 s^{-1}$), the pre-exponential factor that replaces $\frac{A_m S}{A_n N}$ in one case and S/N in the other. The solution of Eq. (30) is given by Eq. (32)

$$I = S' no^2 \exp\left(\frac{-E}{KT}\right) \left\{ 1 + \left(\frac{S'}{\beta}\right) no \int^T \exp\left(\frac{-E}{KT}\right) \mathrm{d}T \right\}^{-2} \qquad (32)$$

It should be emphasized that two cases discussed so far, namely first and second kinetics order, are only special cases in a sense, extreme cases and the general case described by equations Eq. (17) through Eq. (19) may be neither first nor second order even if the simplifying conditions of Eq. (21) are assumed to be general. The resulting Eq. (20) consists of many intermediate cases that do not have a distinct kinetics order. Although, some researchers still attempt to determine for every TL peak a first or second kinetics order [25].

Several attempts [16, 26] have been made to add a third parameter to the two basic ones, the activation energy E and the pre-exponential constant S' (or S), all the attempts extend the "order parameter" implied when talking about first or second-order peak. The order parameters considered so far as a discrete magnitude assuming the value of 1 and 2 can be extended to be a continuous parameter. It is to be noted, however, that the addition of a third parameter is in principle one step in the right direction since the general treatment should include eight parameters ($E, S, A_m, A_n, N, n_o, m_o, n_c$). The best-known way of including the third parameter is that of general kinetics order, b, according to which one can assume that the glow peak is governed by [25].

$$I = \frac{-\mathrm{d}n}{\mathrm{d}t} = S' n^b \exp\left(\frac{-E}{KT}\right) \qquad (33)$$

The kinetics order, b, is normally considered to be between 1 and 2, but it can occasionally exceed this range [13]. The rationale behind writing Eq. (33) is as follows: it is readily seen that a first-order peak is asymmetric, where a second order peak is nearly symmetric. Following Halperin and Braner [19] and Chen [16] we can define the symmetry factor μ_g as:

$$\mu_g = \frac{\delta}{\omega} \qquad (34)$$

where $\delta = T_2 - T_m$, $\omega = T_2 - T_1$ as it is shown in **Figure 7**, and T_1 and T_2 are the low and high temperatures on half- maximum intensity, respectively. It has been
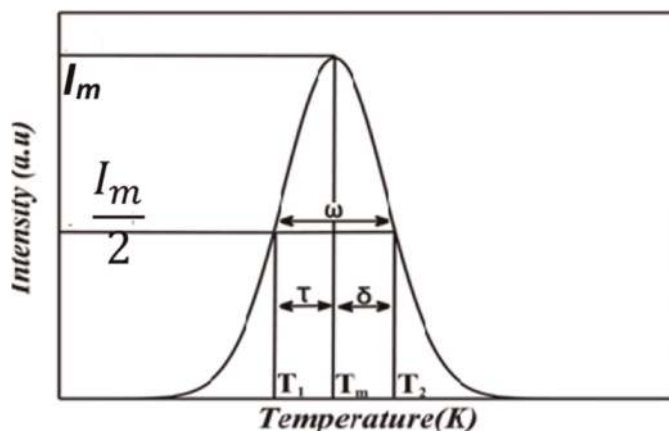
Figure 7.
Parameters used in the calculation of the symmetry factor.

shown [16] that for the first kinetics order, $\mu_g \cong 0.42$ and the second kinetics order, $\mu_g \cong 0.52$.

Of course, intermediate symmetries represented by different values of μ_g are found and the simplest way to present them by taking $1 < b < 2$ in Eq. (30). Chen [16] has shown that μ_g changes from 0.42 to 0.52 as b increasing from 1 to 2. The solution of Eq. (33) for linear heating rate β, is given by:

$$I = Sn_o \, exp\left(\frac{-E}{KT}\right)\left[\frac{(b-1)S}{\beta}\int_{T_o}^{T} exp\left(\frac{-E}{KT}\right)dt + 1\right]^{\frac{-b}{b-1}} \tag{35}$$

where $S = S'n_o^{b-1}$. Eq. (35) represents glow peak intensity according to the general kinetics order.

A few words of caution are in order with respect to this treatment. First, although Eq. (34) has been shown to quite accurately described measured TL peaks [27, 28], it is to be noted that in most cases it is only an empirical presentation and is not based on the three differential equations [Eqs. (17) up to (19)], seem to be more physically significant. However, the general order case is still important because it can handle intermediate circumstances and smooth the first and second-order cases as b_1 and b_2, respectively.

3.1.3 General-order kinetics

May and Partridge supposed the empirical equation that has been suggested to explain the thermoluminescence glow peak if the first or second-order kinetics do not describe the glow peak. The equation is namely the general- order kinetics and written by:

$$I = \frac{n_0 \, s'' \, exp\left(-E/KT\right)}{\left[1 + [(b-1)s''/\beta]\int_{T_0}^{T} exp\left(-E/T' \, K\right)dT'\right]^{b(b-1)}}$$

Hence $s'' = s(Nn_0)$ is called the pre-exponential factor, b the order of kinetics and the rang supposed between 1 and 2 but sometimes this rang has able to be greater than

those. The pre-exponential factor s'' is constant for given the dose, however, it differs with changing the absorbed dose with n_0.

3.1.4 Trap parameters evaluation techniques

3.1.4.1 Empirical methods

We can deduce that the higher the peak temperature T_m, the higher the activation energy Urbach [29], and Urbach [30] found empirically for KCl crystals:

$$E(eV) = \frac{T_m(K)}{500} \tag{36}$$

This can also be written as $E = 23KT_m$ and it differs according to the types of the sample. Halperin [19] deduced $E = 38\ KT_m$ for NACL samples, and Miller and Bube [31] arrived at $E = 39\ KT_m$ for LiF.

The maximum intensity of the peak, according to Randall and Wilkins [12, 13], occurs around the temperature where the electron escape probability is 1 s-1. As a result of Eq. (1), we have:

$$P = S \exp\left(\frac{-E}{KT_m}\right) = 1 \underset{\rightarrow}{\text{yields}} E = KT_m \ln(S) \tag{37}$$

3.1.4.2 Initial rise method

According to Eqs. (6), (12) and (3), we can say that at the start of the glow peak (initial rise region) the TL intensity is proportional to $\exp(-E/kT)$, irrespective of whether the first kinetics order is obeyed or not [32]. This temperature relationship persists until the quantity of trapped electrons is drastically reduced. Hence, by plotting Log (I) versus 1/T, the value of E can be obtained from the slope of the straight line obtained. As a result, using the equation: it is possible to calculate E without knowing the frequency factor S:

$$E = -K \frac{\ln(I)}{\frac{1}{T}} \tag{38}$$

From Eq. (6), we see that when T is slightly greater than T_m, the argument of the second exponential is very small and therefore the value of the exponential function is close to unity and varies very slowly with temperature. The temperature dependence of $I(t)$ is therefore dominated by the first exponential function, however the second exponential function decreases with increasing temperature and at higher temperatures it decreases very rapidly [13].

Therefore, the range of the initial rise must be chosen in which the second exponential function has minimum influence on the TL intensity temperature dependence. Therefore, it is necessary to restrict the temperature range such that the TL intensity does not exceed one-tenth of the maximum intensity [32].

Between temperatures T_1 and T_2 (both $< T_m$) corresponding to values equal to $a_1 I_m$ and $a_2 I_m$ respectively as in **Figure 8**, where:
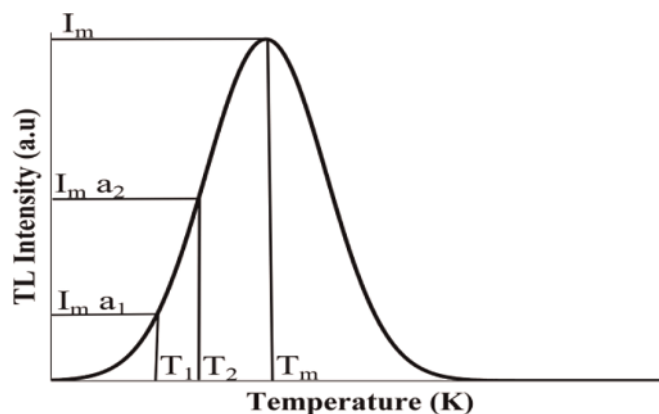
Figure 8.
Extracted parameters from "Christodoulides expression" are to correct the value of the activation energy evaluated by the initial rise method.

$$a_2 \leq 0.5, \quad \frac{a_2}{a_1} \geq 5 \tag{39}$$

On the temperature scale, a series of points were taken at equal intervals and plotted as ln(I) versus (1/T). The value Ec can then be calculated from the slope of the straight line as the energy determined by the initial rise technique; this value is smaller than the real activation energy E by the amount that grows as a_1 and a_2 increase. Christodoulides [33] devised the following expression for the corrected energy E in terms of the measured values E_c, a_1, and a_2:

$$E = (1 + 0.74a_1 + 0.082a_2)E_c - \frac{(2a_1 + 0.22a_2)T_m}{11605} \tag{40}$$

The range of applicability of this equation is restricted by:

$$10 \ll \frac{E}{KT_m} \ll 100 \tag{41}$$

3.1.4.3 Peak shape method

Grossweiner [34] established the first peak shape approach for first-order peaks, writing:

$$E = 1.41K\frac{T_m T_1}{\tau} \tag{42}$$

Where: T_m is the temperature at the maximum intensity, T_1 is the temperature at the half of the maximum intensity in low-temperature side, $\tau = T_m - T_1$ as in **Figure 9**. Grossweiner used the coefficient 1.51, which was later [20] amended to 1.41. Lushchik [35] developed a method for evaluating the activation energy by utilizing the high-temperature half width $\delta = T_2 - T_1$ for first peaks he suggested:
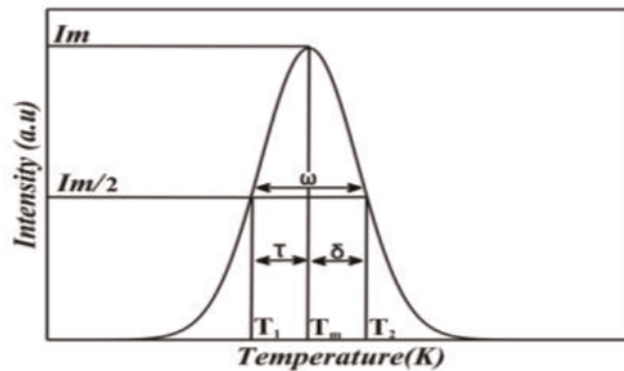
$$E = \frac{KT_m^2}{\delta} \tag{43}$$

Figure 9.
Peak shape method used to calculate the activation energy.

and for second-order peak:

$$E = 2\frac{KT_m^2}{\delta} \tag{44}$$

Chen [16] improved these equations by adding a factor of 0.976 in front of the former and replacing the factor 2 by 1.71 in the latter.

Halperin and Braner [19] have derived their equations for both first [Eq. (45)] and second kinetics orders [Eq. (46)]:

$$E = 1.51K\frac{T_m^2}{\tau} - 3.16KT_m \tag{45}$$

$$E = 1.81K\frac{T_m^2}{\tau} - 4KT_m \tag{46}$$

Chen [16] managed to establish expressions for general kinetics order, which is dependent on the geometry factor of the glow peak which is defined by Eq. (35):

$$E = C_\varphi\frac{KT_m^2}{\varphi} - b_\varphi(2KT_m) \tag{47}$$

Where φ stands for τ, δ, ω and the values of C_φ and b_φ for the three methods are:

$$C_\tau = 3\left(\mu_g - 0.42\right) + 1.51 \tag{48}$$

$$C_\delta = 7.3\left(\mu_g - 0.42\right) + 0.976 \tag{49}$$

$$C_\omega = 10.2\left(\mu_g - 0.42\right) + 2.52 \tag{50}$$

$$b_\tau = 4.2\left(\mu_g - 0.42\right) + 1.58 \tag{51}$$

$$b_\omega = 1 \tag{52}$$

$$b_\delta = 0 \tag{53}$$

where μ_g is geometrical shape factor that equal $\frac{\delta}{\omega}$.

3.1.4.4 Various heating rates method

As mentioned above about Eq. (7), T_m changes with the heating rate β, writing Eq. (7) twice for heating rate β_1 and β_2 with maximum temperatures T_{m1} and T_{m2} we get [36]:

$$E = \frac{kT_{m1}T_{m2}}{T_{m2} - T_{m1}} \left\{ ln\left(\frac{\beta_1}{\beta_2}\right) - ln\left(\frac{T_{m1}^2}{T_{m2}^2}\right) \right\} \qquad (54)$$

The activation energy that will be evaluated from Eq. (54) will be of course in accord with the first kinetics order only. However, Chen and Winer [37], Chen and Kirsh [38] showed that it can be used as a very good approximation for nonfirst-order cases as well.

The maximum condition, Eq. (16), can also take the following form:

$$-ln\left(\frac{\beta}{T_m^2}\right) = \frac{E}{K}\frac{1}{T_m} + ln\left(\frac{E}{SK}\right)$$

According to this equation, Hoogenstraaten [39] suggested using several heating rates, a plot of $ln(\beta/T_m^2)$ vs. $(1/T_m)$ should yield a straight line of slope E/K, so that the activation energy is evaluated. Extrapolation to $1/T_m \to 0$ gives the value of $ln(E/SK)$ from which the frequency factor is immediately found. It was shown that a plot of $ln(I_m)$ versus $1/T_m$ for various heating rates usually yields a straight line too and the activation energy can be extracted similarly. It is to be noted from the theoretical point of view that β should be varied in as board a range as possible. However, this may cause various experimental difficulties. At very low heating rates, the maximum intensity will be low and in fact, the peak smeared, thus not allowing effective extraction of the experimental parameters. At high heating rates, a delay between the sample temperature and that of the measuring device impairs the temperature measurement. Moreover, temperature gradients within the sample usually occur at high heating rates which result in a smearing effect of a different kind. In practice, one should therefore compromise on a relatively narrow range of heating rates [10].

3.1.5 Three points method

A new technique was developed by Rasheedy [25], to evaluate the trap parameters from the measured glow curve according to the general kinetics order.

The behavior of a phosphor's TL intensity is determined by the following equation, [40], for generic kinetics order.

$$I = \frac{-\mathrm{d}n}{\mathrm{d}t} = \frac{n^b}{N^{b-1}} S \exp\left(\frac{-E}{KT}\right) \qquad (55)$$

Where I is the intensity of the TL, n (cm^{-3}), is the electron concentration trapped at time t(s), N (cm^{-3}) is the traps concentration and K (eV/°K) is the Boltzman constant. Eq. (55) is more general than the two equations describing the first and second kinetics orders.

Eq. (55) is a modification of Eq. (33) in which the pre-exponential factor is defined as: $S' = \frac{S}{N^{b-1}}$ instead of $' = \frac{S}{n_o^{b-1}}$. The solution of Eq. (55) is given by Rasheedy [40]:

$$I = \frac{n_o S'' \exp\left(-\frac{E}{KT}\right)}{\left\{1 + \frac{(b-1)S''}{\beta} \int_{T_o}^{T} \exp\left(-\frac{E}{KT}\right)dT\right\}^{\frac{b}{b-1}}} \tag{56}$$

Where the pre-exponential factor $S'' = S(n_o/N)^{b-1}$ which is constant for a given dose but it varies with changes in the absorbed dose, i.e., with n_0.

This method is based on the proportional of the concentration of populated traps during the running of the TL to the area under the glow peak.

I_x is the TL intensity at temperature T_x at any portion of the glow peak as shown in **Figure 10**, then Eq. (55) becomes:

$$I_x = \frac{A_x^b}{N^{b-1}} S \exp\left(\frac{-E}{KT_x}\right) \tag{57}$$

Where A_x is the area under the glow peak between the temperatures T_x and T_f (the final temperature of glow peak). Similarly, we have:

$$I_y = \frac{I_x}{y} = \frac{A_y^b}{N^{b-1}} S \exp\left(\frac{-E}{KT_y}\right) \tag{58}$$

$$I_z = \frac{I_x}{z} = \frac{A_z^b}{N^{b-1}} S \exp\left(\frac{-E}{KT_z}\right) \tag{59}$$

Where I_y and I_z are the TL intensities at temperatures T_y and T_z, respectively. From Eq. (57) and Eq. (58), we shall get

$$E = \left\{ln(y) - bln\left(\frac{A_x}{A_y}\right)\right\}\left[\frac{KT_xT_y}{T_x - T_y}\right] \tag{60}$$

And from Eq. (57) and Eq. (59), we shall get:

$$E = \left\{ln(z) - bln\left(\frac{A_x}{A_z}\right)\right\}\left[\frac{KT_xT_z}{T_x - T_z}\right] \tag{61}$$
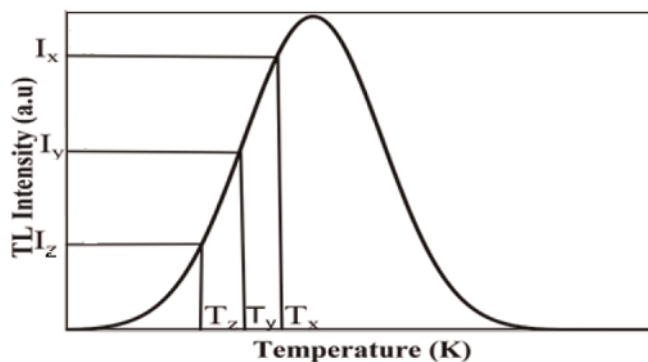

Figure 10.
Three points method used by Rasheedy [25] to investigate the equations used to calculate the trap parameters.

The order of kinetics, b can be obtained using Eqs. (60) and (61) which leads to:

$$b = \frac{T_y[T_x - T_z] \ln(y) - T_z[T_x - T_y] \ln(z)}{T_y[T_x - T_z] \ln\left(\frac{A_x}{A_y}\right) - T_z[T_x - T_y] \ln\left(\frac{A_x}{A_z}\right)} \tag{62}$$

Then, the order of kinetics b can be obtained from Eq. (62). Once the order of kinetics b is determined, the activation energy E(eV) can be determined by using Eq. (60) or Eq. (61).

Since, at $T = T_m$ yields $\frac{\partial I}{\partial T} = 0$

From Eq. (56) and using Eq. (59) leads to the following expression [41]:

$$S'' = \frac{\beta E \, \exp\left(\frac{E}{KT_m}\right)}{\left[bKT_m^2\right] - (b-1)E \exp\left(\frac{E}{KT_m}\right)\int_{T_o}^{T_m} \exp\left(-\frac{E}{KT}\right)dT} \tag{63}$$

A simple analytical method has been developed to obtain the relative value of n_o in the case of general kinetics order [41]:

$$n_o = \frac{I_m \, exp\left(\frac{E}{KT_m}\right)}{\acute{S}} \tag{64}$$

where T_m, and I_m can be obtained from the shape of the glow peak.

Thus, by calculating the kinetics order b, the activation energy E, and the initial trapped electrons number for many points that cover sufficient range on the glow peak, and taking the average value for each parameter, one can determine the trap parameters according to the general kinetics order.

3.1.6 Glow curve analysis (peak shape methods)

A review of the expression used in an intercomparison of glow curve analysis computer programs to evaluate TLD-100 glow curve is given in Ref. [42] where $I(T)$ is written in the following form:

$$I(T) = AS \exp\left(\frac{-E}{KT}\right)\left\{1 + \frac{S(b-1)}{\beta}\int_{T_o}^{T} \exp\left(\frac{-E}{KT}\right)dt\right\}^{\frac{b}{1-b}} \tag{65}$$

where: A = area (counts); b = kinetics order; E = activation energy; I = intensity (counts per s, counts per K); S = frequency factor (s^{-1}).

On the other hand, Eq. (66) is based on first order kinetics which was used by Puchalska, [43], to develop glow-curve analysis software, in the following form:-

$$I(T) = I_m \exp\left(\frac{E}{KT_m} - \frac{E}{KT}\right) \exp\left(\frac{E}{KT_m}\left[\alpha\left(\frac{E}{KT_m}\right)\right]\right.$$

$$\left. -\left(\frac{T}{T_m}\right)\left(\alpha\left(\frac{E}{KT}\right)\right) \exp\left(\frac{E}{KT_m} - \frac{E}{KT}\right)\right) \tag{66}$$

Where the parameter α is defined in Eq. (67) as

$$\alpha(x) = 1 - \frac{a_o + a_1 x + a_2 x^2 + a_3 x^3 + x^4}{b_o + b_1 x + b_2 x^2 + b_3 x^3 + x^4} \tag{67}$$

where the constants a_0, a_1 ... and b_0, b_1 ... are listed in the followings: -

$$a_o = 0.26777 \quad b_o = 3.9584$$

$$a_1 = 8.63476 \quad b_1 = 21.099653$$

$$a_2 = 18.05901 \quad b_2 = 25.63295$$

$$a_3 = 8.573328 \quad b_3 = 9.573322$$

Equation (68) will be used throughout our results which give better fitting to the resultant deconvoluted peaks. Different software was developed by Ratovonjanahary et al. [32], which uses the first kinetics order with an approximation of the second kinetics order. In this software the following equation was used:

$$I(T) = I_m \left\{ \exp 1 + \frac{E}{KT} \frac{T - T_m}{T_m} - \frac{T^2}{T_m^2} \exp\left(\frac{E}{KT} - \frac{T - T_m}{T_m}\right)(1 - \Delta) - \Delta_m \right\} \tag{68}$$

where,

$$\Delta = \frac{2KT}{E}, \Delta_m = \frac{2KT_m}{E}$$

Such a technique was also developed to analyze the glow curve using Eq. (53) by Rasheedy [41], which used the value of the trap parameters obtained by the three points method.

4. Modern clinical applications of TLD

TLD is widely used in various clinical fields for different purposes. The key reasons are undoubtedly their widespread availability, well-studied dosimetric characteristics, and applicability across a broad dose range. Imaging and Radiation Oncology Core-Houston IROC-H conducts remote dosimetry audits on MV photon and electron beams. IROC-H usually used integration between TLD-100 and other dosimetry system like nanoDot or diode systems for achieving the dose commissioning and calibrating dosimetry systems in an acrylic mini-phantom [44]. The failure rate was recorded in dose curves after modeling of the TPS (RayStation-Elekta Inc.) using phantom tests, which was not observed by patient-specific IMRT QA. Such failure was related to little changes in the MLC leaf-tip offset rather than leaf-tip width. Koger and his team [45] in IROC-H prosed four labeled TLD distributed in an anthropomorphic head-and-neck phantom for correcting such failure, (see **Figure 11**). It was utilized a 3D diode array were used in addition to assess the detectability of modeling mistakes [45].

Another crucial issue is to increase the staff's awareness about radiation safety and enhance radiation protection against unnecessary radiation doses. For such purpose, TLD-100 was recently used to validate occupational doses both inside and outside the nuclear
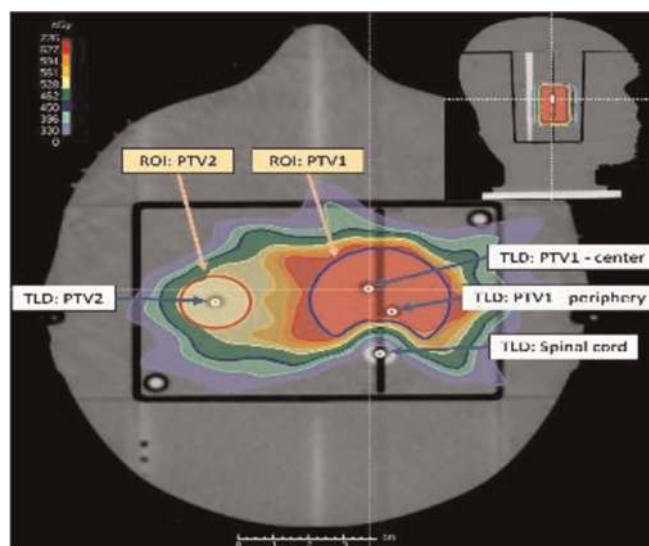
Figure 11.
TLDs were labeled in head-and-neck phantom at IROC-H [45].

medicine department, radiation protection purposes as well as the dose rate distribution around the positron emission tomography or computed tomography (PET/CT) [46].

Some recent studies were envisaged to see how the department compared to reports from other centers across the world in terms of the annual number of procedures and exposure limits, and to see if there was an opportunity for further radiation protection enhancements. As an example, personal TLD was calibrated to estimate the personal equivalent dose Hp (10) and Hp (0.07) at PET/CT. It was used for assessing the employee's exposure [47]. On the other hand, TLD rings personal dosimeters were worn by surgeons in their fingers through sentinel node biopsy procedure to measure personal doses Hp(10) and Hp(0.07), as well as ambiental dose for operating theater and during injection [48]. This will assure that personal equivalent doses are within the acceptable annual determined limits [49].

Other important recent TLD application in diagnostics is using an anthropomorphic phantom that modeled the reference person to get a conversion coefficient connecting dose area product (DAP) to effective patient dosage. They concluded that the effective dosage at the clinical dark-field radiography system, which generates both attenuation and dark-field pictures, is within the range of chest radiography standard dose values [50].

TLDs showed to be an excellent choice for skin dosimetry. Omojola et al. [51] used TLD in measurements of 3D skin dosimetry and verify their results using TPS planning verification at specific spots in the phantom. A full perspective of the dose distribution was achieved; however, they revealed that regions outside the PTV require special attention [52–54].

In addition, in the field of proton therapy, a novel tissue-equivalent TLD-sheet of manganese doped lithium triborate showed a valuable and effective dosimetry technique. It may also be a great in vivo skin dosimetry instrument for proton treatment due to its flexible and reusable properties. Despite the presence of significant energy dependences in the Bragg peak region, the response properties studied in this work, including as reproducibility, fading effects, dosage linearity and dose homogeneity are acceptable [55].

Monte Carlo (MC) simulation is considered a good tool to understand well the TLD [56]. Some algorithm methods based on MC as if pencil beam could be involved in accurate dose in MV radiotherapy calculations. It could be useful to calculate the spectrum inside the detector based on four categories primary photon and electrons and secondary photon and electrons [57].

On the other hand, Low-energy (100 keV) photons (x-rays and gamma) have been widely employed in biological research and medical applications for more than a century, including mammography, fluoroscopy, general radiography, computed tomography, and brachytherapy treatment, among others. The majority of electrons created by low photon energy beams have energies below 10 keV, according to research. The physical processes through which these low-energy electrons interact with matter, on the other hand, are still unknown. Furthermore, it is commonly thought that all energy put within a dosimeter-sensitive volume is converted into a response. However, this assumption could be inaccurate because some of the deposited energy could be utilized to build flaws or damages at the molecular and atomic levels [58].

The hybrid-functional density theory (H-DFT) has shown to be a promising tool for localizing secondary electrons within a dosimeter volume and calculating the energy spent on creating defects or colors centers, among other things, when it comes to the relationship between the energy deposited and the response of a dosimeter. Following that, the quantity of energy that can be truly turned into a dosimeter response following exposure to ionizing radiation would be more accurately determined.

5. Conclusion

The aim of this chapter is concerned with TLD materials, measurements and recent various applications in clinical and industrial fields. TL kinetics are also covered in details due to their importance in knowing traps parameters and band structure-related phenomena that are responsible for TL phenomena. Modern clinical applications of TLD are also covered like quality assurance purposes for proton, x-ray and gamma radiotherapy based on phantom tests. In addition, we shed spot on using TLD for recent accurate methods for skin dose evaluation under IMRT/VMAT radiotherapy. Special attention should be oriented to hybrid-functional density theory Monte Carlo simulation to model TL dosimeters. Recent studies proved a promising tool for localizing secondary electrons within a dosimeter volume and calculating the energy spent on creating defects or colors centers, among other things, when it comes to the relationship between the energy deposited and the response of a dosimeter. Such methods could give knowledge about misunderstanding behaviors of some TLD and could eliminate its disadvantages like missing TL signal or fading; angle and energy of incidence ionizing radiation. In general, the properties of TLD like its inexpensive cost and reusability; easily fabricated, lightweight to wear, readout is simple and can be automated, insensitive to humidity make it advantageous in different clinical and radiation safety applications.

Author details

Hossam Donya[1,2]

1 Faculty of Science, Department of Physics, King Abdulaziz University, Jeddah, Saudi Arabia

2 Faculty of Science, Physics Department, Menoufia University, Shebin El-Koom, Egypt

*Address all correspondence to: hdunia@kau.edu.sa

IntechOpen

References

[1] Furuta Y, Tanaka S. Response of 6LiF and 7LiF thermoluminescence dosimeters to fast neutrons. Nuclear Instruments and Methods. 1972;**104**:36-374

[2] Moreira Ribeiro R, Souza-Santos D. Monte Carlo characterization of an individual albedo neutron monitor. Brazilian Journal of Radiation Sciences. 2021;**9**(2C):1-8. DOI: 10.15392/bjrs.v9i2C.1657

[3] El-Faramawy N, Chopra V, Rawash S, El-Hafez AA, Dhoble SJ. Response of TLD-600/TLD-700 and CR-39 to neutrons for medical dosimetry. Luminescence. 2021;**36**(5):1257-1264

[4] Gibson AB, Piesch E. Technical Reports Series No. 252. Neutron Monitoring for Radiological Protection. Vienna: International Atomic Energy Agency. 1985

[5] ICRU. Determination of Dose Equivalents Resulting from External Radiation Sources. In: Report 39, International Commission on Radiation Protection and Measurements. Bethesda, MD. 1985

[6] Seifert H, Dörschel B, Pawelke J, Hahn T. Comparison of calculated and measured neutron sensitivities of an electret albedo dosemeter. Radiation Protection Dosimetry. 1991;**37**(1):13-18

[7] Seifert H, Dorschel B, Pawelke J. Neutron dosimetry using an electret albedo dosimeter. In: 1991 Proceedings 7th International Symposium on Electrets (ISE 7). London: IEEE; 1991. pp. 753–758

[8] Fellinger J, Hahn T, Henniger J, Hübner K, Schmidt P. Fast neutron sensitivity of TL detectors using proton radiator techniques. Isotopenpraxis Isotopes in Environmental and Health Studies. 1991;**27**(7):342-346. DOI: 10.1080/10256019108622562

[9] El-Adawy A, Khaled NE, El-Sersy AR, Hussein A, Donya H. TL dosimetric properties of Li2O–B2O3 glasses for gamma dosimetry. Applied Radiation and Isotopes. 2010;**68**(6):1132-1136

[10] Polymeris GS, Çoskun S, Tsoutsoumanos E, Konstantinidis P, Aşlar E, Şahiner E, et al. Dose response features of quenched and reconstructed, TL and deconvolved OSL signals in BeO. Results in Physics. 2021;**25**:104222

[11] Begum M, Rahman AM, Abdul-Rashid HA, Yusoff Z, Nawi SN, Khandaker MU, et al. Photonic crystal fibre as a potential medium for radiotherapy dosimetry. Applied Radiation and Isotopes. 2021;**174**:109771

[12] Saray AA, Kaviani P, Shahbazi-Gahrouei D. Dosimetric characteristics of lithium triborate (LiB3O5) nanophosphor for medical applications. Radiation Measurements. 2021;**140**:106502

[13] Horowitz YS, Yossian D. Computerised glow curve deconvolution: Application to thermoluminescence dosimetry. Radiation Protection Dosimetry. 1995;**60**(1):1-114

[14] Randall JT, Wilkins MHF. Phosphorescence and electron traps II. The interpretation of long-period phosphorescence. Proceedings of the Royal Society of London. Series A. Mathematical and Physical Sciences. 1945;**184**(999):390-407

[15] Garlick GFJ, Wilkins MHF. Short period phosphorescence and electron traps. Proceedings of the Royal Society of

London. Series A. Mathematical and Physical Sciences. 1945;**184**(999):408-433

[16] Chen R. On the calculation of activation energies and frequency factors from glow curves. Journal of Applied Physics. 1969;**40**(2):570-585

[17] Wrzesińska A. Their production and thermoluminescence curves. Acta Physica Polonica. 1956;**15**:151

[18] Adirovitch EI. La formule de Becquerel et la loi élémentaire du déclin de la luminescence des phosphores cristallins. Journal de Physique et le Radium. 1956;**17**(8-9):705-707

[19] Halperin A, Braner AA, Ben-Zvi A, Kristianpoller N. Thermal activation energies in NaCl and KCl crystals. Physical Review. 1960;**117**(2):416

[20] Dussel GA, Bube RH. Theory of thermally stimulated conductivity in a previously photoexcited crystal. Physical Review. 1967;**155**(3):764

[21] Saunders IJ. The thermally stimulated luminescence and conductivity of insulators. Journal of Physics C: Solid State Physics. 1969;**2**(12):2181

[22] De Muer D. Development of a universal method for calculating the thermoluminescence parameters. Physica. 1970;**48**(1):1-12

[23] Bräunlich P, Kelly P, Fillard JP. Thermally stimulated luminescence and conductivity. In: Thermally Stimulated Relaxation in Solids. Berlin, Heidelberg: Springer; 1979. pp. 35-92

[24] Moharil SV. On the general-order kinetics in thermoluminescence. Physica Status Solidi A: Applications and Materials Science. 1982;**73**(2): 509-514

[25] Rasheedy MS. A new evaluation technique for analyzing the thermoluminescence glow curve and calculating the trap parameters. Thermochimica Acta. 2005;**429**(2): 143-147

[26] May CE, Partridge JA. Thermoluminescent kinetics of alpha-irradiated alkali halides. The Journal of Chemical Physics. 1964;**40**(5):1401-1409

[27] Prokić M. Analysis of the thermoluminescence glow curves of natural barite. Journal of Physics and Chemistry of Solids. 1977;**38**(6):617-622

[28] De Blasi C, Gallassini S, Manfredotti C, Micocci G, Ruggiero L, Tepore A. Trapping levels in PbI2. Solid State Communications. 1978;**25**(3):149-153

[29] Urbach R. Zur lumineszenz der alkalihalogenide. Sitzungsberichte Akad. der Wiss. Wien. 1930;**139**:363-372

[30] Urbach F. Storage and Release of Light by Phosphors. Vol. 115. New York: John Wiley and Sons; 1948

[31] Miller LD, Bube RH. Luminescence, trapping, and F centers in lithium fluoride crystals. Journal of Applied Physics. 1970;**41**(9):3687-3697

[32] Ratovonjanahary AJF, Raboanary R, Andriambololona R. Quartz Glow-Peaks Lifetime Analysis: TL Glow-Curve Deconvolution Functions for First Order of Kinetic Compared to Initial Rise Method. In: HEPMAD 04 Conference, Madagascar, 27 Sep-01 Oct. 2004

[33] Christodoulides C. Errors involved in the determination of activation energies in TL and TSDC by the initial rise method. Journal of Physics D: Applied Physics. 1985;**18**(8):1665

[34] Grossweiner LI. A note on the analysis of first-order glow curves. Journal of Applied Physics. 1953;**24**(10): 1306-1307

[35] Lushchik CB. The investigation of trapping centers in crystals by the method of thermal bleaching. Soviet Physics Jetp-USSR. 1956;**3**(3):390-399

[36] Booth AH. Calculation of electron trap depths from thermoluminescence maxima. Canadian Journal of Chemistry. 1954;**32**(2):214-215

[37] Chen R, Winer SAA. Effects of various heating rates on glow curves. Journal of Applied Physics. 1970;**41**(13): 5227-5232

[38] Chen R, Kirsh Y. Analysis of Thermally Stimulated Process. Oxford: Pergamon Press; 1981

[39] Hoogenstraaten W. Electron traps in zinc sulphide phosphors. Philips Research Reports. 1958;**13**:515-693

[40] Rasheedy MS. On the general-order kinetics of the thermoluminescence glow peak. Journal of Physics: Condensed Matter. 1993;**5**(5):633

[41] Rasheedy MSRMS. A complete system for obtaining the trap parameters of thermoluminescence glow peak. Japanese Journal of Applied Physics. 1996;**35**(2R):634

[42] Bos AJJ, Piters TM, Gómez-Ros JM, Delgado A. An intercomparison of glow curve analysis computer programs: I. Synthetic glow curves. Radiation Protection Dosimetry. 1993;**47**(1-4): 473-477

[43] Puchalska M, Bilski P. GlowFit—A new tool for thermoluminescence glow-curve deconvolution.

Radiation Measurements. 2006;**41**(6): 659-664

[44] Alvarez P, Kry SF, Stingo F, Followill D. TLD and OSLD dosimetry systems for remote audits of radiotherapy external beam calibration. Radiation Measurements. 2017;**106**: 412-415

[45] Koger B, Price R, Wang D, Toomeh D, Geneser S, Ford E. Impact of the MLC leaf-tip model in a commercial TPS: Dose calculation limitations and IROC-H phantom failures. Journal of Applied Clinical Medical Physics. 2020;**21**(2): 82-88

[46] Nilsson I, Himmelman J, Khan J, Dalmo J. The potential to use Tld measurements to validate the occupational radiation protection at the Department of Nuclear Medicine. Radiation Protection Dosimetry. 2021; **195**(3-4):355-362

[47] Pavičar B, Davidović J, Petrović B, Vuleta G, Trivić S, Šajinović V, et al. Nuclear medicine staff exposure to ionising radiation in 18F-FDG PET/CT practice: A preliminary retrospective study. Arhiv za Higijenu Rada i Toksikologiju. 2021;**72**(3):216-223

[48] Petrovic B, Vicko F, Radovanovic D, Samac J, Tot A, Radovanovic Z, et al. Occupational radiation dose of personnel involved in sentinel node biopsy procedure. Journal of Medical Physics. 2021;**91**:117-120

[49] Ali W, Sulieman A, Tamam N, Boshara N, Aldhebaib A, Alkhorayef M, et al. Estimation of patients organ doses and staff exposure during bone scan examination. Radiation Physics and Chemistry. 2021;**188**:109693

[50] Frank M, Urban T, Willer K, Noichl W, De Marco F, Schick R, et al.

Dosimetry on first clinical dark-field chest radiography. Medical Physics. 2021;**48**(10):6152-6159

[51] Omojola AD, Akpochafor MO, Adeneye SO, Akala IO, Agboje AA. Chest X-rays of newborns in a medical facility: Variation between the entrance skin dose measurements using the indirect and direct methods for clinical dose audit. Japanese Journal of Radiology. 2021;**40**(2):1-7

[52] Moradi F, Khandaker MU, Mahdiraji GA, Ung NM, Bradley DA. Dose mapping inside a gamma irradiator measured with doped silica fibre dosimetry and Monte Carlo simulation. Radiation Physics and Chemistry. 2017;**140**:107-111

[53] Moradi F, Ung NM, Mahdiraji GA, Khandaker MU, Entezam A, See MH, et al. Angular dependence of optical fibre thermoluminescent dosimeters irradiated using kilo- and megavoltage X-rays. Radiation Physics and Chemistry. 2017;**135**:4-10

[54] Moradi F, Mahdiraji GA, Dermosesian E, Khandaker MU, Ung NM, Mahamd Adikan FR, et al. Influence of dose history on thermoluminescence response of Ge-doped silica optical fibre dosimeters. Radiation Physics and Chemistry. 2017;**134**:62-70

[55] Kato T, Sagara T, Komori S, Kato R, Takeuchi A, Narita Y. Dosimetric properties of a newly developed thermoluminescent sheet-type dosimeter for clinical proton beams. Journal of Applied Clinical Medical Physics. 2021;**22**(4):158-165

[56] Donya H, Seniwal B, Darwesh R, Fonseca TC. Prospective Monte Carlo simulation for choosing high efficient detectors for small-field dosimetry. In:

Theory, Application, and Implementation of Monte Carlo Method in Science and Technology. London: IntechOpen; 2019

[57] Donya H. Pencil-beam fluence evaluation based on Monte Carlo simulations algorithm of high energetic treatment photons. Journal of Medical Signals and Sensors. 2018;**8**(2):81

[58] Massillon-JL G. Future directions on low-energy radiation dosimetry. Scientific Reports. 2021;**11**:10569. DOI: 10.1038/s41598-021-90152-3